Mineralogical Magazine, February 2009, Vol. 73(1), pp. 17–26

Preferred ion diffusion pathways and activation energies for Ag in the crystal structure of stephanite, Ag_5SbS_4

M. Leitl[1,2], A. Pfitzner[2] and L. Bindi[3,*]

[1]BASF Construction Chemicals GmbH, Dr.-Albert-Frank-Straße 32, D-83308 Trostberg, Germany
[2]Institut für Anorganische Chemie, Universität Regensburg, Universitätsstrasse 31, D-93040, Regensburg, Germany
[3]Museo di Storia Naturale, Sezione di Mineralogia, Università degli Studi di Firenze, Via La Pira, 4, I-50121, Firenze, Italy

[*Received 21 January 2009; Accepted 26 March 2009*]

ABSTRACT

The crystal structure of stephanite from the type locality, Freiberg District, Saxony, Germany, was refined in the space group $Cmc2_1$, up to a final R index of 0.0427. Unit-cell parameters are: a 7.8329(6) Å, b 12.458(1) Å, c 8.5272(7) Å, V 832.1(1) Å^3; $Z = 4$. The previously reported structural model is confirmed, but a higher-precision refinement was achieved herein by the introduction of third-order non-harmonic Gram-Charlier tensors for one Ag atom. In the structure of stephanite, Sb forms isolated SbS_3 pyramids, which typically occur in sulphosalts, and Ag occupies sites with coordination ranging from triangular to almost tetrahedral. Both the Sb–S and Ag–S bond distances closely match the values commonly observed in the structures of other Ag sulphosalts and sulphides.

The use of non-harmonic parameters for Ag allowed a better description of the electron density related to Ag, which is usually difficult to refine in good ionic conductors. A careful analysis of the energy barriers between the Ag sites defines preferred ion-diffusion pathways within the crystal structure of stephanite. The diffusion of Ag ions occurs preferentially along the sites Ag1 and Ag2, giving rise to two-dimensional nets of Ag atoms in which the ion conduction probably takes place.

Keywords: stephanite, crystal-structure refinement, non-harmonic approach, Ag, diffusion pathway, ionic conductivity.

Introduction

Bindi and Evain (2007) showed that the non-harmonic approach, based upon a Gram-Charlier development of the atomic displacement factors, can be useful in mineral sciences for the determination of unknown structures. Such an approach is used to refine already known structures with suspiciously high R values and/or high isotropic displacement parameters for Ag or Cu atoms. The non-harmonic approach has been used successfully over the past twenty years to solve numerous structures of non-conducting materials (van der Lee *et al.*, 1993; Boucher *et al.*, 1994; Gaudin *et al.*, 1997) and ion-conducting phases (Kuhs and Heger, 1979; Boucher *et al.*, 1992, 1993; Haile *et al.*, 1997; Evain *et al.*, 1998; Haile and Wuensch, 2000*a*,*b*,*c*). Recently, it has been used to solve complex structures of natural and synthetic sulphosalts and the pearceite-polybasite mineral family: (Evain *et al.*, 2006*a*,*b*; Bindi *et al.*, 2006*a*,*b*, 2007); fettelite, (Bindi *et al.*, 2009); synthetic skinnerite, (Pfitzner, 1998); synthetic tetrahedrite, (Pfitzner *et al.*, 1997).

We have reinvestigated the crystal structure of stephanite, Ag_5SbS_4, which was determined previously by Ribár and Nowacki (1970) in the space group $Cmc2_1$. Although their structural model is correct, Ribár and Nowacki reported an R value of 9.4% (photographic methods) and B_{iso} values of 3.82, 4.49 and 3.33 Å^2 for the Ag1, Ag2

* E-mail: luca.bindi@unifi.it
DOI: 10.1180/minmag.2009.073.1.17

and Ag3 positions, respectively (approximately up to three times the values observed for Sb and for the S atoms). The non-harmonic approach, based upon a Gram-Charlier development of the atomic displacement factors, has been applied here to determine whether or not the crystal-structure refinement previously reported by Ribár and Nowacki (1970) can be improved upon and to provide information on the diffusion pathways of Ag, which are related to the fast ion conduction character of stephanite.

X-ray crystallography and crystal-structure refinement

The two samples containing the stephanite crystals that were used in the present study (sample STP_01: Museo di Storia Naturale, Sezione di Mineralogia, Università di Firenze, Italy – catalogue number 2363/G; sample STP_02: Mineralogische Staatssammlung, München, Germany – catalogue number 51164) are from Freiberg, Saxony, Germany, a well known source of Ag-bearing minerals. In both samples, stephanite occurs as black anhedral to subhedral grains up to 400 μm long and shows a grey-black to black streak. The other mineral spatially associated with stephanite is calcite.

The crystal STP_01 was analysed by means of an Oxford Diffraction Xcalibur 3 diffractometer (Mo-$K\alpha$ radiation, λ = 0.71073 Å) fitted with a Sapphire 2 CCD detector, whereas STP_02 was analysed using a STOE-IPDS diffractometer using graphite-monochromatized Mo-$K\alpha$ radiation. Nearly identical unit-cell dimensions were found for the two crystals investigated. For this reason, crystal STP_02, which displayed a better diffraction quality, was chosen for subsequent studies. In anticipation of the presence of possible twinning, which is common in stephanite, special care was taken on the choice of the fraction of reciprocal space covered. A relatively high $\sin(\theta)/\lambda$ cut off and a high redundancy were chosen in the recording setting design. Intensity integration and standard Lorentz-polarization correction were performed with the *X-RED* program package (Stoe and Cie, 1997). Subsequent calculations were conducted with the *Jana2000* program suite (Petříček *et al.*, 2000), except for the optimization of the crystal shape and dimension, which were performed with *X-shape* (Stoe and Cie, 1997), based on the *Habitus* program (Herrendorf, 1993). Full-matrix refinements were carried out on F^2, with all reflections included.

Starting with the model obtained for the structure of stephanite by Ribár and Nowacki (1970), the refinement in the $Cmc2_1$ space group smoothly converged to a residual R = 0.0538 value for 998 reflections [$I > 3\sigma(I)$] and 62 parameters. To mimic the spread of electrons associated with Ag along diffusion paths, third-order non-harmonic Gram-Charlier tensors for the Ag2 atom were used for the Debye-Waller description (Johnson and Levy, 1974; Kuhs, 1984). All stephanite crystals are systematically twinned on {110}, which are repeated to form pseudo-hexagonal groups (e.g. Gaines *et al.*, 1997). A schematic visualization of this partially merohedric twinning is given in Fig. 1. For the refinement, the twin matrix |0.43 1.43 0/0.56 −0.43 0/0 0 −1| was used. The refinement showed that the ratio of the second twin domain was only 9%. This small twin fraction is one of the reasons for the good quality of the X-ray diffraction data set and the successful absorption correction, which is usually critical in the case of twinned crystals. At the last stage, the residual value settled at R = 0.0427 for 998 independent observed reflections [$3\sigma(I)$ level] and 62 parameters, and at R = 0.0466 for all 1041 independent reflections.

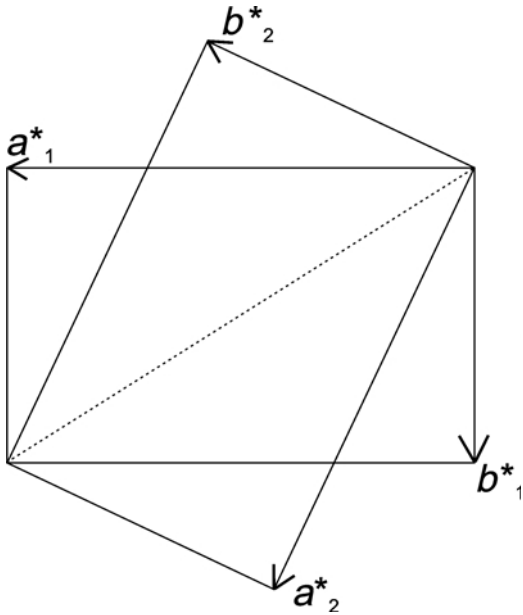

FIG. 1. Schematic visualization in the reciprocal space of the twinning of stephanite. The twin parts are indexed by 1 and 2. The discontinuous line shows the twinning plane.

Crystal characteristics, data collection and reduction parameters, and refinement results are given in Table 1. Atomic parameters are reported in Tables 2, 3 and 4, whereas structure factors (Table 5) have been deposited with the Principal Editor of *Mineralogical Magazine* and are available from www.minersoc.org/pages/e_journals/dep_mat_mm.html.

Chemical composition

A preliminary chemical analysis using energy dispersive spectrometry, performed on the same crystal fragments used for the structural study, did not indicate the presence of elements ($Z > 9$) other than Ag, Sb and S. Since the unit-cell parameters of the two crystals were nearly identical, the chemical composition was then determined on the sample STP_01, which is the larger and better polished crystal, using wavelength dispersive analysis (WDS) by means of a Jeol JXA-8600 electron microprobe. Major and minor elements were determined at an accelerating voltage of 20 kV and a probe current of 40 nA, for 30 s count time. The following X-ray lines were used for the WDS analyses: Ag-$L\alpha$, Sb-$L\beta$, and S-$K\alpha$.

TABLE 1. Crystallographic data and experimental details for STP_02.

Molar (mass/gmol^{-1})	789.1
Crystal colour	Grey
Crystal system	Orthorhombic
Space group	$Cmc2_1$ (Nr. 36)
Lattice parameters	
a (Å)	7.8329(6)
b (Å)	12.458(1)
c (Å)	8.5272(7)
Volume (Å^3)	832.1(1)
Z	4
ρ_{calc} (g cm^{-3})	6.3
Diffractometer	STOE-IPDS
Radiation	Mo-$K\alpha$, λ =0.71073 Å
Monochromator	Graphite crystal
Angles (º), $\Delta\varphi$ (º)	0.0−280.5, 1.5
Absorption correction	numeric, X-RED and X-SHAPE (Stoe and Cie, 1997)
μ(Mo) (mm^{-1})	15.65
Temperature (K)	293
2θ range (º)	3.8 − 56.3
hkl range	$-10 \leqslant h \leqslant 10$; $-16 \leqslant k \leqslant 16$; $-11 \leqslant l \leqslant 11$
Number of reflections	5362
Independent reflections	1041
Independent reflections [$I > 3\sigma(I)$]	998
$R\sigma$	0.0344
R_{int}	0.0632
Refinement	Full-matrix least-squares on F^2
Software	*Jana2000* (Petříček *et al.*, 2000)
Weighting scheme	σ, 0.03
Extinction coefficient	0.068(6) (Becker and Coppens, 1974)
R_1 [$I > 3\sigma(I)$]	0.0427
$wR2$ [$I > 3\sigma(I)$]	0.1106
R_1 (all)	0.0466
wR_2 (all)	0.1125
Refined parameters	62
Goodness of Fit [$I > 3\sigma(I)$]	1.53
Goodness of Fit (all)	1.54
Twin ratio	0.91(1):0.09(1)
ρ_{max} (eÅ^{-3})	2.24
ρ_{min} (eÅ^{-3})	−1.64

TABLE 2. Wyckoff positions, atomic coordinates and isotropic displacement parameters U_{eq} (Å^2) for STP_02.

Atoms	Wyckoff	*x*	*y*	*z*	U_{eq}
Sb1	4*a*	0	0.82095(7)	0.5143	0.0305(2)
Ag1	8*b*	0.1856(1)	0.12312(9)	0.6010(2)	0.0508(3)
Ag2	8*b*	0.3139(4)	0.0648(3)	0.2849(3)	0.0676(4)
Ag3	4*a*	½	0.8549(1)	0.4456(3)	0.0587(5)
S1	4*a*	½	0.0276(3)	0.5917(4)	0.0335(8)
S2	4*a*	0	0.0142(2)	0.4096(4)	0.0305(8)
S3	8*b*	0.7706(3)	0.7670(2)	0.3464(3)	0.0326(6)

The estimated analytical precision is ±0.75 wt.% Ag, ±0.15 wt.% Sb, and ±0.20 wt.% S. The standards employed were Ag – pure element (Ag), Sb – pure element (Sb), and S – pure element (S). The STP_01 crystal was found to be homogeneous within analytical error. The average chemical composition (six analyses on different spots) is 68.30 wt.% Ag, 15.44 wt.% Sb, and 16.23 wt.% S. On the basis of 10 atoms, the formula can be written as $Ag_{5.00}Sb_{1.00}S_{4.00}$.

Results and discussion

Description of the structure

The crystal structure of stephanite contains two anionic parts: sulphide ions (S1 site) and complex anionic $(SbS_3)^{3-}$ units (S2 and S3 sites). The Sb atoms are in a three-fold coordination occupying the top of a pyramid with 3 S making a base. SbS_3 polyhedra are isolated from each other (Fig. 2) and show a sum of bonding angles of 285.7° for S–Sb–S, and a mean Sb–S distance of 2.438 Å (Table 6). The latter value is consistent with that observed for pyrargyrite, $Ag_3[SbS_3]$ (2.452 Å, Engel and Nowacki, 1966), and with those observed for different polytypes of polybasite (2.418–2.452 Å, Bindi *et al.*, 2007; Evain *et al.*, 2006*a*). The $(SbS_3)^{3-}$ units exhibit a 'layer-like' arrangement along the *c* axis (Fig. 3). A small sideway tilt of the units can be seen. This means that the basal face of a pyramid, which is set up by three S atoms, is tilted with respect to the *ab* layer. Between the different layers the tilt orientation changes with a layer distance of *z*/2, which is due to the space-group symmetry of stephanite.

Each S atom of the SbS_3 units (S2, S3) is coordinated by four Ag atoms with distances in the range 2.523–2.894 Å (Table 6). The sulphide ions (S1) are located in the centre of a triangle defined by three $(SbS_3)^{3-}$ units of one layer and are separated from the thioantimonate units by seven Ag sites at distances less than 3.1 Å. All three Ag sites in stephanite are coordinated by S atoms at distances between 2.483 Å and 3.030 Å (Table 6), which are common values for Ag thioantimonates and Ag sulphides in general. Figure 4 shows the distorted tetrahedral coordination of Ag1 and Ag2, whereas Ag3 is planar coordinated by three S atoms. Silver atoms separate the anionic units from one another.

TABLE 3. Anisotropic-displacement parameters (Å^2) for STP_02.

Atom	U_{11}	U_{22}	U_{33}	U_{12}	U_{13}	U_{23}
Sb1	0.0323(4)	0.0323(4)	0.0268(4)	0	0	0.0009(3)
Ag1	0.0559(5)	0.0576(6)	0.0389(5)	–0.0102(4)	–0.0004(3)	–0.0109(4)
Ag2	0.0670(7)	0.0750(8)	0.0609(7)	0.0197(6)	0.0101(5)	–0.0239(6)
Ag3	0.0512(7)	0.0577(8)	0.067(1)	0	0	–0.0184(7)
S1	0.033(1)	0.038(2)	0.030(2)	0	0	0.005(1)
S2	0.031(1)	0.030(1)	0.031(2)	0	0	0.001(1)
S3	0.0324(9)	0.031(1)	0.034(1)	–0.0050(8)	–0.0029(9)	0.0020(9)

TABLE 4. Higher-order displacement parameters C_{ijk} (multiplied by 10^3) for Ag2 in STP_02.

C_{111}	C_{112}	C_{113}	C_{122}	C_{123}
0.008(1)	0.0046(5)	0.0046(6)	0.0041(3)	0.0036(3)
C_{133}	C_{222}	C_{223}	C_{233}	
0.0033(5)	0.0025(4)	0.0032(3)	0.0024(4)	

Preferred ion diffusion pathways and activation energies for Ag

The atom site Ag2 was refined by using non-harmonic parameters of third order according to Gram-Charlier (Zucker and Schulz, 1982). When using conventional anisotropic displacement parameters for Ag2, the refinement converged at an $R1$ value of 0.06 and with a $wR2$ value of ~0.13. A comparison between both refinement strategies concerning Ag2 can be seen in Fig. 5. Basically, the use of non-harmonic parameters shows the interaction between the Ag atom and the surrounding S atoms. Errors for the third-order deformation tensors were calculated by a Monte-Carlo approach (Pfitzner *et al.*, 1997) in order to show the significance of the non-harmonic deformation. The errors for the deformation are <10% of the maximum deformation values. The space filling of the Ag2 site is significantly reduced in the direction pointing to the S sites S1 and S3 (Fig. 5*b*). A second symmetry-equivalent S1 atom at a distance of 3.030 Å shows a substantially smaller influence on the non-harmonic distribution function of Ag. In general, differences from the common ellipsoidal way of describing the displacement of an atom can be observed. A careful analysis of the pathways of Ag diffusion in the crystal structure of stephanite showed that, in contrast to the pyrargyrite structure (Leitl, 2007), a connection exists between the distances between the sites of Ag, and the activation energy. Several short Ag–Ag distances range from 2.90 to 3.05 Å. A second group of metal distances ranges from 3.25 to 3.50 Å. A larger distance of >3.8 Å is present between Ag1 and Ag3. Along the latter direction,

TABLE 6. Selected bond distances (Å) and angles (º) for STP_02.

Ag1–Ag1	2.907(1)	S1–Ag3–S3	122.81(6)
Ag1–Ag2	2.968(3)	S2–Ag1–S3	88.9(1)
Ag1–Ag2	2.991(3)	S2–Ag1–S3	152.76(8)
Ag1–S1	2.736(2)	S2–Ag2–S3	91.59(13)
Ag1–S2	2.574(3)	S2–Sb1–S3	95.19(8)
Ag1–S3	2.894(3)	S3–Ag3–S3	113.7(1)
Ag1–S3	2.523(3)	S3–Sb1–S3	95.28(8)
Ag2–Ag2	2.916(4)	S2–Sb1–S3	95.19(8)
Ag2–S1	2.483(4)	S3–Ag1–S3	104.76(8)
Ag2–S2	2.751(3)	Sb1–S2	2.451(3)
Ag2–S3	2.596(4)	Sb1–S2–Ag1	105.1(1)
Ag3–S1	2.486(4)	Sb1–S2–Ag2	110.7(1)
Ag3–S3	2.532(3)	Sb1–S3 (x2)	2.431(2)
Ag3–S3	2.532(3)	Sb1–S3–Ag1	86.04(8)
S1–Ag2–S2	132.4(2)	Sb1–S3–Ag1	102.12(9)
S1–Ag2–S3	131.3(2)	Sb1–S3–Ag2	109.9(1)
S1–Ag1–S2	105.09(9)	Sb1–S3–Ag3	106.3(1)
S1–Ag1–S3	92.29(9)		
S1–Ag1–S3	97.9(1)		

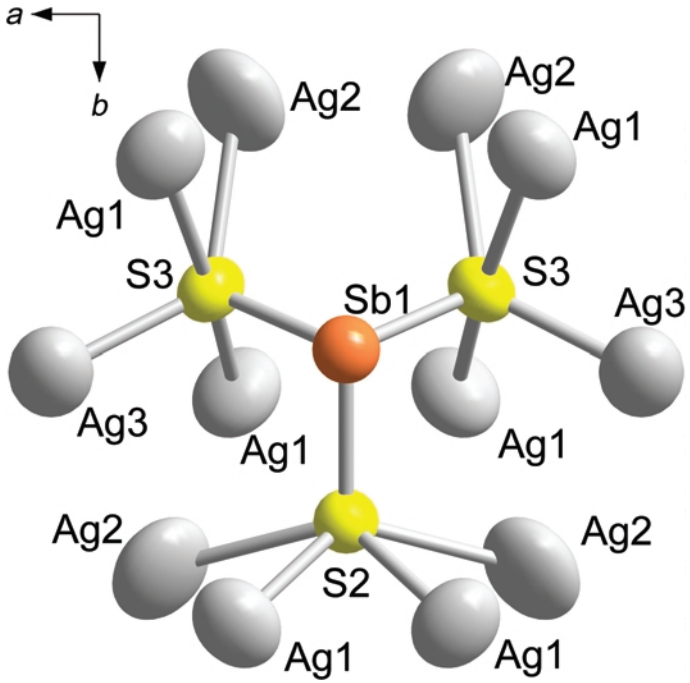

FIG. 2. The connection between the AgS_n-polyhedra and the SbS_3 pyramid in the crystal structure of stephanite.

the greatest activation energy of almost 1.0 eV is obtained, which is necessary for the Ag atom to jump to the next noble metal site. With smaller Ag−Ag distances, the One Particle Potentials (OPPs) decrease. For the Ag sites with intermediate atomic distances, the OPPs are between 0.5 and 0.65 eV. The lowest potential for activating a Ag atom to jump to its next position is present between two Ag2 sites at a distance of 2.916 Å with a value of 0.4 eV, which is a commonly observed value for Ag site distances close to 3.0 Å. The shortest noble metal distance

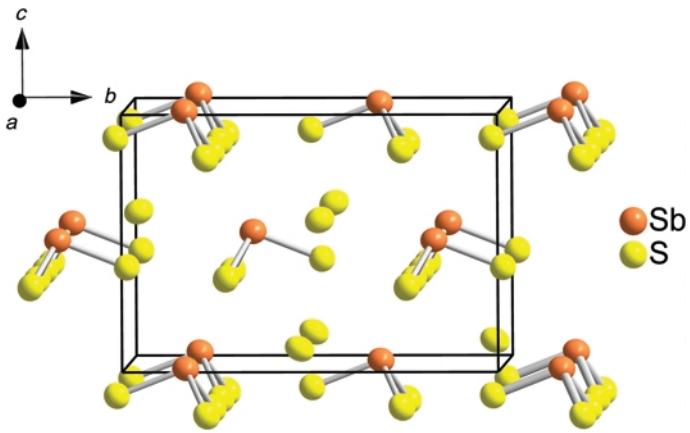

FIG. 3. Arrangement of the $(SbS_3)^{3-}$ units and the sulphide ions in the crystal structure of stephanite along the *a* axis.

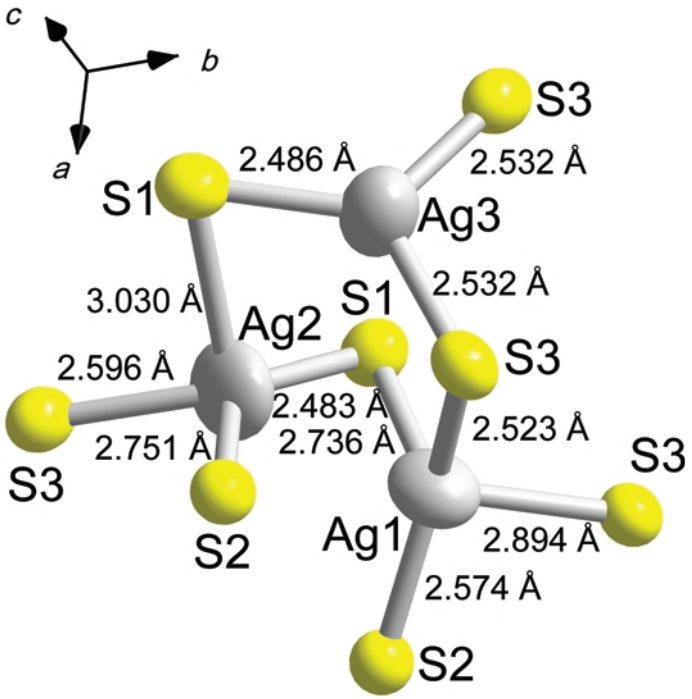

FIG. 4. Coordination of the Ag atoms in the crystal structure of stephanite.

of 2.907 Å is present between two Ag1 sites, but here the activation energy is 0.5 eV. We observed values of 0.45 and 0.7 eV for the energy barriers between Ag1 and Ag2 at distances of 2.991 and

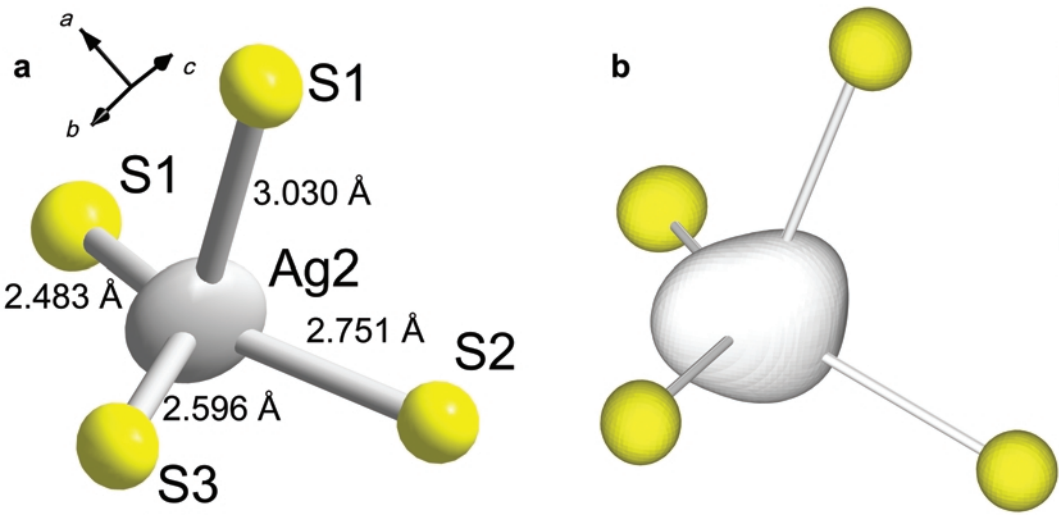

FIG. 5. Coordination of the Ag2 site in stephanite. Comparison between conventional anisotropic refinement (*a*) and non-harmonic refinement using JPDF maps (*b*). The non-harmonic probability distribution is drawn at 90% probability levels for the S atom and 99% for the Ag atoms. Four S atoms coordinate the Ag atom in a 3 + 1 coordination.

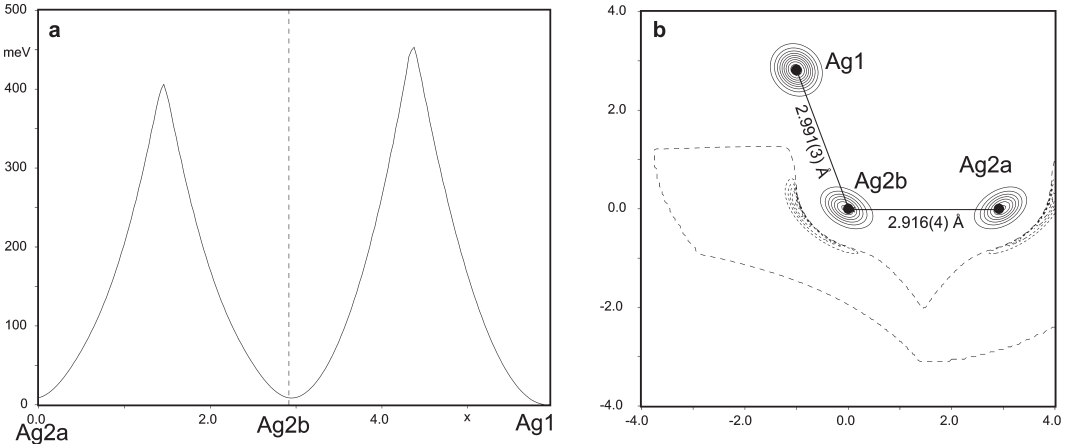

FIG. 6. The OPP and JPDF analysis of several Ag sites in stephanite. (*a*) Energy barriers in meV along the diffusion pathways with the lowest activation energies. Diffusion path along the line given in (*b*). (*b*) JPDF map of the Ag sites in stephanite that are separated by the diffusion pathways with the lowest activation energies. Ag2 has been visualized based on non-harmonic parameters. The full lines show the probability density function values in increments of 0.591 $Å^{-3}$. Dashed lines show areas of negative probability density function values in increments of 0.0001 $Å^{-3}$. The maximum and minimum probability density values are 5.91 and −0.0005 $Å^{-3}$, respectively.

2.968 Å, respectively. The two-dimensional JPDF (Joint Probability Density Function) maps and the corresponding route-depending activation energies between the atom sites with the lowest particle potential are shown in Fig. 6. After an analysis of the energy barriers between the Ag sites, the preferred ion diffusion pathways within the crystal structure of stephanite can be defined. The charge transport by Ag ions occur preferentially along pathways with low activation energy, which in this case are the routes along the sites Ag1 and Ag2 with distances of ~3.0 Å. If these

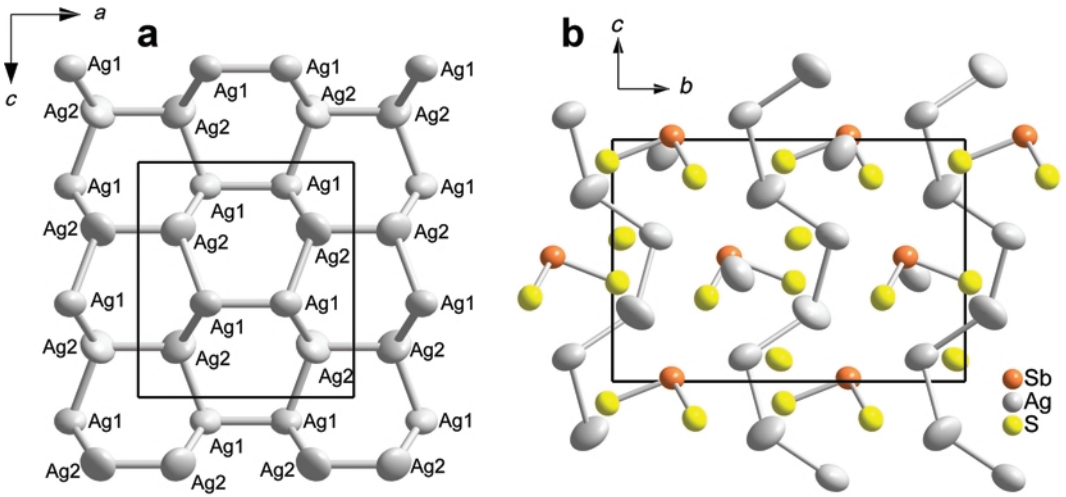

FIG. 7. Preferred diffusion pathways of the Ag atoms in stephanite. The energy barriers between the connected Ag sites range from 0.4 to 0.5 eV. Larger interatomic distances for Ag are connected with higher energy barriers. (*a*) A puckered net of Ag sites in the *ac*-layer with interatomic distances less than 3.1 Å. (*b*) Lateral view on the nets of Ag sites. No direct contact between the layers is present.

routes are visualized in the crystal structure by lines, puckered two-dimensional nets of Ag atoms form, in which the ion conduction preferably takes place. Figure 7 shows these nets arranged parallel to the *ac*-layer that are not connected to one another. A charge exchange between these layers must happen by participation of the Ag3 site and energy barriers that are higher than 0.5 eV. Impedance spectroscopic investigations (Leitl, 2007) resulted in an activation energy of 0.35 eV for stephanite. This value is in good agreement with the calculated energy barriers.

Acknowledgements

The paper benefited from the reviews by Emil Makovicky and Paul Spry. Associate Editor Elena Sokolova is thanked for her efficient handling of the manuscript. We thank Dr R. Hochleitner (Mineralogische Staatsammlung, München, Germany) for providing us with one stephanite sample. LB acknowledges the M.I.U.R., P.R.I.N. 2007 project 'Complexity in minerals: modulation, phase transition, structural disorder' grant issued to Silvio Menchetti.

References

Becker, P.J. and Coppens, P. (1974) Extinction within the limit of validity of the Darwin transfer equations. I. General formalism for primary and secondary extinction and their applications to spherical crystals. *Acta Crystallographica A*, **30**, 129–147.

Bindi, L. and Evain, M. (2007) Gram-Charlier development of the atomic displacement factors into mineral structures: The case of samsonite, $Ag_4MnSb_2S_6$. *American Mineralogist*, **92**, 886–891.

Bindi, L., Evain, M. and Menchetti, S. (2006*a*) Temperature dependence of the silver distribution in the crystal structure of natural pearceite, $(Ag,Cu)_{16}(As,Sb)_2S_{11}$. *Acta Crystallographica B*, **62**, 212–219.

Bindi, L., Evain, M., Pradel, A., Albert, S., Ribes, M. and Menchetti, S. (2006*b*) Fast ionic conduction character and ionic phase-transitions in disordered crystals: The complex case of the minerals of the pearceite-polybasite group. *Physics and Chemistry of Minerals*, **33**, 677–690.

Bindi, L., Evain, M. and Menchetti, S. (2007) Complex twinning, polytypism and disorder phenomena in the crystal structures of antimonpearceite and arsenpolybasite. *The Canadian Mineralogist*, **45**, 321–333.

Bindi, L., Keutsch, F.N., Francis, C.A. and Menchetti, S. (2009) Fettelite, $[Ag_6As_2S_7][Ag_{10}HgAs_2S_8]$ from Chañarcillo, Chile: Crystal structure, pseudosymmetry, twinning, and revised chemical formula. *American Mineralogist*, **94**, 609–615.

Boucher, F., Evain, M. and Brec, R. (1992) Single-crystal structure determination of γ-Ag_8SiTe_6 and powder X-ray study of low-temperature α and β phases. *Journal of Solid State Chemistry*, **100**, 341–355.

Boucher, F., Evain, M. and Brec, R. (1993) Distribution and ionic diffusion path of silver in γ-Ag_8GeTe_6: A temperature dependent anharmonic single crystal structure study. *Journal of Solid State Chemistry*, **107**, 332–346.

Boucher, F., Evain, M. and Brec, R. (1994) Second-order Jahn-Teller effect in $CdPS_3$ and $ZnPS_3$ demonstrated by a non-harmonic behaviour of Cd^{2+} and Zn^{2+} d^{10} ions. *Journal of Alloys and Compounds*, **215**, 63–70.

Engel, P. and Nowacki, W. (1966) Die Verfeinerung der Kristallstruktur von Proustit, Ag_3AsS_3, und Pyrargyrit, Ag_3SbS_3. *Neues Jahrbuch für Mineralogie Monatshefte*, 181–195.

Evain, M., Gaudin, E., Boucher, F., Petříček, V. and Taulelle, F. (1998) Structures and phase transitions of the A_7PSe_6 (A=Ag,Cu) argyrodite-type ionic conductors. I. Ag_7PSe_6. *Acta Crystallographica B*, **54**, 376–383.

Evain, M., Bindi, L. and Menchetti, S. (2006*a*) Structural complexity in minerals: twinning, polytypism and disorder in the crystal structure of polybasite, $(Ag,Cu)_{16}(Sb,As)_2S_{11}$. *Acta Crystallographica B*, **62**, 447–456.

Evain, M., Bindi, L. and Menchetti, S. (2006*b*) Structure and phase transition in the Se-rich variety of antimonpearceite, $(Ag_{14.67}Cu_{1.20}Bi_{0.01}Pb_{0.01}Zn_{0.01}Fe_{0.03})_{15.93}(Sb_{1.86}As_{0.19})_{2.05}(S_{8.47}Se_{2.55})_{11.02}$. *Acta Crystallographica B*, **62**, 768–774.

Gaines, R.V., Skinner, H.C.W., Foord, E.E., Mason, B. and Rosenzweig, A. (1997) *Dana's New Mineralogy*. Eighth Edition. John Wiley & Sons, New York, USA.

Gaudin, E., Fischer, L., Boucher, F., Evain, M. and Petříček, V. (1997) $Ag_2Ti_2P_2S_{11}$: A new layered thiophosphate. Synthesis, structure determination and temperature dependence of the silver distribution. *Acta Crystallographica B*, **53**, 67–75.

Haile, S.M. and Wuensch, B.J. (2000*a*) X-ray diffraction study of $K_3NdSi_7O_{17}$: a new framework silicate with a linear Si–O–Si bond. *Acta Crystallographica B*, **56**, 773–779.

Haile, S.M. and Wuensch, B.J. (2000*b*) Structure, phase transitions and ionic conductivity of $K_3NdSi_6O_{15}{\cdot}xH_2O$. II. Structure of β-$K_3NdSi_6O_{15}$. *Acta Crystallographica B*, **56**, 349–362.

Haile, S.M. and Wuensch, B.J. (2000*c*) Structure, phase transitions and ionic conductivity of $K_3NdSi_6O_{15}{\cdot}xH_2O$. I. α-$K_3NdSi_6O_{15}{\cdot}2H_2O$ and its

polymorphs. *Acta Crystallographica B*, **56**, 335–348.

Haile, S.M., Wuensch, B.J., Laudise, R.A. and Maier, J. (1997) Structure of $Na_3NdSi_6O_{15}.2H_2O$ – a layered silicate with paths for possible fast-ion conduction *Acta Crystallographica B*, **53**, 7–17.

Herrendorf, W. (1993) *Habitus*. PhD dissertation, University of Karlsruhe, Germany.

Johnson, C.K. and Levy, H.A. (1974) Pp. 311–336 in: *International Tables for X-ray Crystallography*, (J.A. Ibers and W.C. Hamilton, editors). Vol. IV, Kynoch Press, Birmingham, UK.

Kuhs, W.F. (1984) Site-symmetry restrictions on thermal-motion-tensor coefficients up to rank 8. *Acta Crystallographica A*, **40**, 133–137.

Kuhs, W.F. and Heger, G. (1979) Pp. 233–236 in: *Fast Ion Transport in Solids* (P. Vashishta, J.N. Mundy and G.K. Shenoy, editors), Elsevier, Amsterdam.

Leitl, M. (2007) *Strukturchemische und impedanzspektroskopische Untersuchungen an silberionenleitenden Substanzen, Münzmetallthiophosphaten und Kupferargyroditen*. PhD thesis, Universität Regensburg, Institut für Anorganische Chemie, 228 pp.

Petříček, V., Duek, M. and Palatinus, L. (2000) *JANA2000, a crystallographic computing system*. Institute of Physics, Academy of Sciences of the Czech Republic, Prague, Czech Republic.

Pfitzner, A. (1998) Disorder of Cu^+ in Cu_3SbS_3: structural investigations of the high- and low-temperature modification. *Zeitschrift für Kristallographie*, **213**, 228–236.

Pfitzner, A., Evain, M. and Petříček, V. (1997) $Cu_{12}Sb_4S_{13}$: A temperature dependent structure investigation. *Acta Crystallographica B*, **53**, 337–345.

Ribár, B. and Nowacki, W. (1970) Die Kristallstruktur von Stephanit, $[SbS_3|S|Ag_5^{III}]$. *Acta Crystallographica B*, **26**, 201–207.

Stoe and Cie (1997) *X-RED* (version 1.09), *STOE Data Reduction Program*; X-shape (version 1.02), Crystal Optimisation for Numerical Absorption correction, Darmstadt, Germany.

Van der Lee, A., Boucher, F., Evain, M. and Brec, R. (1993) Temperature dependence of the silver distribution in $Ag_2MnP_2S_6$ by single crystal X-ray diffraction. *Zeitschrift für Kristallographie*,, **203**, 247–264.

Zucker, U.H. and Schulz, H. (1982) Statistical approaches for the treatment of anharmonic motion in crystals. I. A comparison of the most frequently used formalisms of anharmonic thermal vibrations. *Acta Crystallographica A*, **38**, 563–568.